Published in final edited form as:
*Biochemistry*. 2010 May 4; 49(17): 3619–3630. doi:10.1021/bi100199q.

# Phosphorylation of the Transcription Factor Ets-1 by ERK2: Rapid Dissociation of ADP and Phospho-Ets-1

**Kari Callaway**[1,5], **William F. Waas**[1,2], **Rainey Mark A**[1,3], **Pengyu Ren**[4], and **Kevin N. Dalby**[1,2,3,4,5,*]

[1]Division of Medicinal Chemistry, University of Texas at Austin, TX 78712, USA

[2]Graduate Programs in Pharmacy, University of Texas at Austin, TX 78712, USA

[3]Graduate Programs in Cell and Molecular Biology, University of Texas at Austin, TX 78712, USA

[4]Graduate Programs in Biomedical Engineering, University of Texas at Austin, TX 78712, USA

[5]Graduate Programs in Biochemistry, University of Texas at Austin, TX 78712, USA

## Abstract

ERK2 a major effector of the BRAF oncogene is a promiscuous protein kinase that has a strong preference to phosphorylate substrates on Ser-Pro or Thr-Pro motifs. As part of a program to understand the fundamental basis for ERK2 substrate recognition and catalysis we have studied the mechanism by which ERK2 phosphorylates the transcription factor Ets-1 on Thr-38. A feature of the mechanism in the forward direction is a partially rate-limiting product release step, $k_{off}$ = 59 ± 6 $s^{-1}$, which is significant, because in order to approach maximum efficiency substrates for ERK2 may evolve to ensure that ADP dissociation is rate-limiting. To further understand the mechanism of product release, the binding of the products to ERK2 was assessed and the reaction was examined in the reverse direction. These studies demonstrated that phospho-Ets-1 (*p*-Ets) binds > 20-fold more tightly to ERK2 than ADP ($K_d$ = 7.3 and 165 μM respectively), revealed that the products exhibit little interaction energetically, while bound to ERK2 and that they can dissociate ERK2 in a random order. The overall equilibrium for the reaction in solution ($K_{eq}$ = 250 $M^{-1}$) was found to be similar to that while bound to the enzyme ($K_{int}$ = 525 $M^{-1}$). To determine what limits $k_{off}$ several pre-steady-state experiments were performed. A catalytic trapping approach furnished a rate-constant of $k^{a}_{-ADP}$=61 ± 12 $s^{-1}$ for the dissociation of ADP from the abortive ternary complex, ERK2•Ets•ADP. To examine *p*-Ets dissociation the binding of a fluorescent derivative (*p*-Ets-*F*), which binds ERK2 with similar affinity to *p*-Ets, was examined by stopped-flow kinetics. Using this approach *p*-Ets-*F* was found to bind through a single-step mechanism, with the following parameters, $k_{-p\text{-Ets-}F}$ = 121 ± 3.8 $s^{-1}$ and $k_{p\text{-Ets-}F} = 9.4 \pm 0.3 \times 10^6$ $M^{-1}s^{-1}$. Similar results were found in the presence of saturating ADP. These data suggest that $k_{off}$ may be limited by the dissociation of both products and are consistent with the notion that Ets-1 has evolved to be an efficient substrate for ERK2, where ADP release is, at least, partially rate-limiting. A molecular mechanics model of the complex formed between ERK2 and residues 28–138 of Ets-1 provides insight into the role of substrate docking interactions.

---

The therapeutic potential of targeting the Ras pathway has been recognized (1–5), and could be the single most important mitogenic pathway in human cells, contributing to more than 30% of all known cancers (6). Ras, a GTPase, is anchored to the cytoplasmic face of the plasma membrane and is activated by a cascade of events following various hormones binding to their

*Corresponding author: Kevin N. Dalby Division of Medicinal Chemistry, College of Pharmacy, University of Texas at Austin, 78712, USA. Tel. 512-4719267 Fax. 512-2322606 Dalby@mail.utexas.edu.

respective cell surface receptors. Unregulated signaling from growth factor receptors, and oncogenic forms of Ras and the Ras effector protein kinase Raf (7–12) lead to sustained ERK1/2 activity, which results in the unrestricted activation of signals that control cell survival and/or progression into the S-phase of the cell cycle (13,14). A recent study identified mutant RAS and BRAF in cancer cell lines of various origins and showed that BRAF oncogenic mutations occur in approximately 8% of human cancers, being particularly common in melanoma, colon cancer and non small lung carcinoma (15).

ERK1/2 are remarkable enzymes, each displaying an ability to efficiently phosphorylate a subset of Ser/Thr-Pro motifs residing on various cellular proteins. Notably, they display an ability to discriminate against many accessible Ser/Thr-Pro motifs, while rapidly phosphorylating others. Specificity of ERK1/2 for their substrates is achieved, in part, through the utilization of remote recruitment sites. For example, ERK2 has two recruitment sites that are used to bind short peptide motifs (16) called the D-recruitment site (DRS)[1] and the F-recruitment site (FRS) (please see Figure 1A).

While the importance of the DRS and FRS in recognizing ERK2 substrates is well-established general principles governing mechanisms of substrate recognition and turnover by ERK2 remain to be elucidated. For example, there is no clear understanding of the relationships between docking interactions at the recruiting sites and events, such as phosphorylation, that occur within the active site. It is also not known whether all docking interactions function through similar mechanisms.

To address some of these questions we examined the mechanism of phosphorylation of the transcription factor Ets-1 (which lacks a conventional D and F site) by ERK2, using residues 1–138 as a surrogate of the full-length protein.[2] The *N*-terminus (residues 1–39) of Ets-1 is disordered, while residues 40–138, which contain a sterile alpha motif (SAM) domain (18), form a five-helix bundle, with helix 1 beginning immediately *C-terminal* to the phosphorylation site Thr-38 (Figure 1B).[3] ERK2 catalyzes the phosphorylation of Ets-1 on Thr-38 with remarkable specificity (19, 20). Structure/function studies suggest that both the *N*-terminus and the SAM domain of Ets-1, but not the Thr-Pro motif, contribute to the formation of the ERK2-Ets complex (21, 22), thereby bringing Thr-38 to within close proximity of the active site, to facilitate phosphorylation of Thr-38, through a mechanism termed proximity-induced catalysis (23).[4] This mechanism was proposed, because Ets binds unactivated ERK2 (which lacks the ability to bind the Thr-Pro motif) with similar affinity to activated ERK2 (21). Furthermore, mutation of Pro-39 to bulky or charged residues has no significant effect on the affinity of the Ets protein for ERK2 in the absence and presence of an ATP analog

[1]*Abbreviations:* BSA, bovine serum albumin fraction V; DTT, dithiothreitol; EDTA, ethylene diamine tetraacetic acid; EGTA, ethylene glycerol-bis [2-aminoethyl ether]-N,N,N'N'-tetraacetic acid; IAA, Iodoacetamide; TPCK, tosylphenylalanylchloromethane; HEPES, N-(2-hydroxyethyl)-piperazine-N'-2-ethanesulfonic acid; TRIS, Tris (hydroxymethyl) aminomethane; IPTG, isopropyl-β-D-thiogalactopyranoside; PMSF, phenylmethylsulfonyl fluoride; TFA, trifluoroacetic acid; ERK, extracellular signal-regulated protein kinase; Ets, murine ($His_6$-tagged) Ets-1 (1–138); *p*-Ets, murine ($His_6$-tagged) Ets-1 (1–138) phosphorylated on Thr-38; *p*-Ets-*F*, murine ($His_6$-tagged) Ets-1 (1–138) containing a single Cys residue at position 31 labeled with 5'-iodoacetamidofluorescein phosphorylated on Thr-38; MAPK, mitogen-activated protein kinase; PCR, polymerase chain reaction; ESI, electrospray ionization; DRS, D-recruitment site; FRS, F-recruitment site; MKK1G7B, constitutively active recombinant human mitogen-activated protein kinase kinase 1 (ΔN4/S218D/M219D/N221D/S222D) where ΔN4 indicates a deletion of residues 32–43; SAM domain, sterile alpha motif domain.

[2]Residues 1–138 of Ets-1, which we term Ets for convenience, is an excellent model for the full-length Ets-1 protein with respect to its recognition and phosphorylation by ERK2 (17).

[3]An NMR-derived structure of Ets was recently updated as PDB 2JV3 in the protein data bank.

[4]MAP kinases phosphorylate substrates within a consensus sequence, φ-χ-Ser/Thr-θ, where φ corresponds to a small hydrophobic residue (often proline), χ corresponds to any amino acid, and θ corresponds to proline. Recognition of the consensus sequence by the MAPK is mediated by *intrinsic interactions* mainly involving the activation segment of the MAPK. However, according to the mechanism of proximity-induced catalysis the consensus sequence of Ets-1 neither contributes binding energy, nor interacts intimately with the active site of ERK2 in the ground state ternary complex. Rather the ternary complex is stabilized exclusively by interactions extrinsic to the active site, which are often termed docking interactions.

(23). These results suggest that the binding of the Thr-Pro motif in the active site of ERK2 is not essential for complex formation.

Kinetic studies revealed that the turnover of Ets-q by ERK2 is governed by two partially rate-limiting steps, which are attributed to the phosphorylation of Ets-q on the enzyme ($k_p$ = 106 ± 8 $s^{-}$) and the process of product release ($k_{off}$ = 59 ± 6 $s^{-}$) (Scheme 1) (24). Here we examine the mechanism of product release in more detail to address whether this step is limited by the dissociation of ADP or phospho-Ets. This study is significant, because it addresses the notion that substrates for a promiscuous protein kinase such as ERK2 likely evolve to rapidly dissociate once phosphorylated. To address the mechanism, the reaction was examined using a combination of steady-state and pre-steady-state kinetics.

## EXPERIMENTAL PROCEDURES

### Preparation of Proteins

The expression of MKK1G7B, ERK2, Ets, and Ets-*F* and the activation of ERK2 by MKK1G7B have been reported (21).

**Phosphorylation of Ets and Ets-F—**Purified Ets or Ets-*F* (20 μM) was incubated with active ERK2 (5 nM) at 27 °C in 50 mM HEPES pH 7.4, 100 mM KCl, 2 mM DTT, 0.1 mM EDTA, 0.1 mM EGTA, 40 μg/mL BSA, 10 mM $MgCl_2$, and 2 mM ATP (3 mL buffer/1 mg protein) for 2 hrs. The reaction was stopped with 10 mM EDTA and the ATP was removed by dialysis in 20 mM Tris pH 8.0, 0.1% (*v*/*v*) β-mercaptoethanol, and 0.3% (by mass) Brij-30. Following dialysis, the protein was purified by anion exchange chromatography on a Mono-Q HR 10/10 column that was developed with a gradient of 0–500 mM NaCl over 17 column volumes. After the protein was eluted at 250 mM NaCl, the selected fractions were combined and dialyzed in 25 mM HEPES pH 7.5, 50 mM KCl, 2 mM DTT, 0.1 mM EDTA, and 0.1 mM EDTA. The phosphorylation of Ets and Ets-*F* was confirmed by ESI mass spectrometry following elution (0–100% acetonitrile, 80 minutes, 0.6 mL/min) from a reverse phase C18 Vydac column (218TP54, 25 cm × 4 mm).

### Molecular Biology

A bacterial expression vector, NpT7-5 encoding a hexa-histidine tag followed by cDNA encoding the rat ERK2 (NpT7-5 $His_6$-ERK2, a gift of N. Ahn, University of Colorado, Boulder, Colorado), was modified by PCR using site-directed mutagenesis to construct K229T/H230D ERK2. The NpT7-5 $His_6$-ERK2 vector was digested with SacII and HindIII and ligated into a SacII-HindIII digested pBluescript (pBS) vector using T4 DNA ligase to create pBSERK2. The mutations were produced by a two-step PCR reaction using the following conditions: 94 °C for 5 min to denature the complementary strands; 30 cycles of 55 °C for 30 sec to anneal the primers, extension for 1 min at 72 °C, followed by a denaturation step at 94 °C for 45 sec; complementary strands were extended a final 10 min at 72 °C. The first round of PCR generated two overlapping products, fragment A and B, from two separate reactions using pBS-ERK2 as template. Fragment A was amplified using an outer forward primer that contained an EcoRI restriction site (underlined) (5'-TAT GTT GAA TTC CAA GGG TTA TAC-3') and an inner reverse primer containing the mutation (*italics*) for K229T/H230D (5'-CTG GTC AAG GTA GTC *GGT TCC* TGG GAA GAT-3'). Fragment B was amplified with an inner forward primer containing the mutation for K229T/H230D (5'-ATC TTC CCA *GGA ACC* GAC TAC CTT GAC CAG-3'), and an outer reverse primer containing the beginning of the HindIII restriction site in ERK2 (5'-GGT CGA CGG TAT CGA TAA GC-3'). Fragments A and B were purified and used as templates for a second round of PCR using only the outer primers. The product was digested with EcoRI and HindIII and ligated into EcoRI-HindIII digested pBS-ERK2. The pBSERK2 mutants were digested with SacII and HindIII and subcloned into SacII-HindIII

digested NpT7-5 His6-ERK2. All mutations were verified by sequencing the DNA at UT core facilities.

## Ligand-Binding

**Isothermal Titration Calorimetry—**Prior to the experiment, active ERK2 was dialyzed into 25 mM HEPES pH 8.0, 100 mM KCl, 2 mM β-mercaptoethanol, and 20 mM $MgCl_2$. To ensure that the buffer was identical, the dialysis buffer was then used to make the MgADP solution. The concentration of the MgADP solution was such that a 2.5 molar ratio of MgADP to active ERK2 was reached in the cell upon the last injection. Titrations were carried out on a MCS titration calorimeter (Microcal, Inc.) at 27 °C in 25 mM HEPES pH 8.0, 100 mM KCl, 2 mM β-mercaptoethanol, and 20 mM $MgCl_2$. ADP was titrated into 263 μM ERK2 with one 2 μl injection followed by twenty-five 10 μl injections with a 5 sec injection duration followed by 240 sec between injections. Control experiments used the same buffer as the experiments, but were done in the absence of ERK2. The data resulting from the control experiment was subtracted from the experimental data using the Origin 2.3 data analysis software. This same software was used for integrations and fitting to a simple one-binding site model. The data fitting process produced values for the binding stoichiometry (n), association constant ($K_a$ ), and the molar enthalpy change (ΔH).

**Fluorescence Anisotropy Binding Assays—**Assays were performed as previously described (21).

## Kinetic Experiments

**Steady-state kinetic experiments in the reverse direction[5]—**Reactions were carried out at 27 °C in kinase assay buffer (25 mM HEPES pH 7.4, 100 mM KCl, 2 mM DTT, 40 μg/mL BSA, and 20 mM $MgCl_2$) containing 50 nM ERK2 and varied concentrations of [$^{32}$P] *p*-Ets (1.8–90 μM) and ADP (100–5000 μM). Rates were measured under conditions where total product formation represented less than 10% of the initial substrate concentrations. The reaction was incubated for 10 min before initiation by addition of enzyme. Aliquots (8 μl) were taken at time points and applied to a 20 × 20 cm silica gel thin-layer chromatography (TLC) plate (Sigma, St. Louis, MO). TLC plates were developed in TLC eluent (300 mM ammonium acetate, 366 mM HCl, and 20% (v/v) methanol) and exposed to Phosphor screens (Molecular Dynamics). The amount of [γ-$^{32}$P] ATP formed was determined using the program ImageQuant (Molecular Dynamics) and calibrating with a sample of known specificity. Initial rates were determined by linear least squares fitting to plots of product against time. The kinetic constants were obtained using the program Scientist (Micromath) by fitting the data to equation 1 by global fitting.

$$k_{obs} = \frac{k_{cat}\,[ADP]\,[p-Ets]}{K_m^{ADP}K_m^{p-Ets} + K_m^{p-Ets}\,[ADP] + K_m^{ADP}\,[p-Ets] + [ADP]\,[p-Ets]} \qquad \text{(eqn. 1)}$$

[5]*Steady-state kinetic terms:* $k_{cat}^{f}$, $k_{cat}^{r}$, catalytic constants for forward and reverse reactions respectively; $K_m^{ADP}$, $K_m^{ATP}$, $K_m^{Ets}$, $K_m^{p-Ets}$, Michaelis-Menton constants for ADP, ATP, Ets and phospho-Ets respectively; $K_d^{ADP}$, $K_d^{p-Ets}$, dissociation constant for the dissociation of ADP and phospho-Ets from $E^{ADP}$ and $E_{p\text{-}Ets}$ respectively; $K_i^{ATP}$, $K_i^{Ets}$ inhibition constant for ATP and Ets respectively; $k_p$ and $k_{-p}$, first-order rate constants for the inter-conversion of the $E_{Ets}^{ATP}$ and $E_{p-Ets}^{ADP}$ ternary complexes in the forward and reverse direction respectively; $K_{eq}$ equilibrium constant for the forward reaction between ATP and Ets in solution; $K_{int}$ equilibrium constant for the forward reaction between ATP and Ets while bound to ERK2.

**Rapid Chemical Quench[6]—**Rapid quench experiments were performed on a Kintek RQF-3 rapid-quench flow apparatus. Reactions were conducted at 27 °C in 25 mM HEPES (pH 8.0), 50 mM KCl, 2 mM DTT, and 20 mM $MgCl_2$. Experiments were initiated by the rapid mixing of solution A (containing ERK2) with an equal volume of solution B (containing other reagents, including ATP). After brief time intervals (2–100 msec), reactions were quenched with 115 μl of 2 M $H_3PO_4$. The quenched reaction mixture was collected in 1.5 mL centrifuge tubes and centrifuged briefly at 5000 x *g*. Aliquots (50 μl) of the quenched reaction mixture were spotted on P81 paper. The papers were washed first in 50 mM $H_3PO_4$ (3 × 10 min) and then in acetone (3 × 1 min). After the papers were dry, the amount of *p*-Ets was determined by counting the associated c.p.m. on a scintillation counter. Data were fitted by global fitting by numerical integration to the appropriate kinetic model using the program KinTek Explorer Pro (25,26).

**Fluorescence Stopped-Flow—**Stopped-flow measurements were performed on a Kintek SF 2001 Airforce 1 air-driven stopped-flow apparatus. To establish the dead time, the fluorescent quenching of N-acetyl-tryptophanamide by N-bromosuccinimide was monitored (28). For the Kintek SF 2001 Airforce 1 stopped-flow instrument, a dead time of 2 msec was determined. Experiments were conducted at 27 °C using a 530 nm band pass filters with a 25 nm bandwidth (Corion). An excitation wavelength of 492 nm was used. A 200 nM solution of *p*-Ets-*F* in 25 mM HEPES pH 7.5, 50 mM KCl, 2 mM DTT, 40μg/mL BSA, 0.1 mM EDTA, and 0.1 mM EGTA was reacted with solutions of ERK2 (1–40 μM) in the same buffer. The solutions were incubated at 27 °C for 3 minutes before being mixed to give a final concentration of 100 nM *p*-Ets-*F* and 0.5–20 μM ERK2. The reaction was monitored for a total of 30 msec and an average of 4–5 traces was used for data analysis. Data were fitted by numerical integration to the appropriate kinetic model using the program KinTek Explorer Pro (25,26).

## Computational Procedures

**Modeling for ERK2-Ets 28–138 interactions—**The complex structure of active ERK2 (PDB ID: 2ERK) and Ets (PDB ID: 2JV3) was predicted using the molecular mechanics modeling approaches available in the TINKER software package (29). An OPLS-AA force field (30) was used to represent atomic interactions. Regular unphosphorylated Thr and Tyr residues replaced the phosphorylated Thr and Tyr residues in 2ERK. The two molecules were first separated apart by 40 Å, with the ERK2 active site facing the Ets *N*-terminus. The potential smoothing (PSS) method (31) was then used to "dock" the two proteins into a complex by minimizing the total system energy. During the energy minimization, ERK2 was kept rigid, and so was Ets except for the *N-terminal* residues 29–53. In order to allow for backbone conformational changes in the *N-terminal* segment of Ets, residues 29–53 of Ets were divided into rigid bodies comprised of backbone amides and side chain groups (i.e. each residue containing two rigid bodies). In PSS, a smoothing parameter of 20 was utilized, with 100 steps in the smoothing schedule. Energy minimization ceased when the energy gradient dropped below 0.1 kcal/mol per degree of freedom. The non-bonded interactions were cutoff at 30 Å. A dielectric constant of 5 was used. To facilitate the search for optimal complex structure, a flat bottom restraint was applied between the $C_\beta$ atom of Thr-38 in Ets and the Cγ of Asp-147 in ERK2. The restraint ($K_r$ = 2.0 kcal/mol/Å$^2$ worked to loosely pull the two atoms into each other's proximity (2 to 6 Å).

[6]*Pre-steady-state kinetic terms*: $k_{off}$, first-order rate constant for the formation of E from $E^{ADP}_{p-Ets}$; $k_{-ADP}$ first-order rate constant for the dissociation of ADP from $E^{ADP}$; $k^a_{-ADP}$, first-order rate constant for the dissociation of ADP from the abortive complex $E^{ADP}_{Ets}$; $k_{-p\text{-Ets}}$, first-order rate constant for the dissociation of *p*-Ets from $E_{p-Ets}$; $k_{+p\text{-Ets}}$ second-order rate constant for the association of *p*-Ets and ERK2; $k_{-p\text{-Ets-}F}$ first-order rate constant for the dissociation of *p*-Ets-*F* from $E_{p-Ets-F}$; $k_{+p\text{-Ets-}F}$ second-order rate constant for the association of *p*-Ets-*F* and ERK2; $k_s$ rate constant for the recombination of substrates with free ERK2.

The PSS-minimized structure was then subjected to atomic energy minimization (without the rigid body constraint) using GBSA implicit solvent model. The conformation of the $^{38}$Thr-Pro$^{39}$ motif is inferred from the known conformation of the peptide substrate in the CDK active site (PDBID: 1QMZ). To take advantage of this known conformation, additional restraints were applied to force the $^{38}$Thr-38-Pro$^{39}$ motif to adopt the corresponding backbone torsion angles found in the CDK2•peptide complex in 1QMZ, and also to push the Pro-39 into the hydrophobic pocket behind phospho-Tyr-185 of ERK2. The overall structural change (RMSD) caused by this minimization is less than 0.5 Å, mostly in the Ets *N*-terminus where the restraints were applied. The effect on the ERK2-Ets interface away from the active site was negligible. All restraints were then removed for another fully atomic energy minimization, in which all degrees of freedom were set free, again in the GBSA implicit solvent.

### Analytical Procedures

**Electrospray ionization mass spectrometry of proteins and peptides—**Proteins and tryptic peptides were analyzed by an electrospray ion trap mass spectrometer (LCQ, Finnigan MAT, San Jose, CA) coupled on-line with a microbore HPLC (Magic 2002, Michrom BioResources, Auburn, CA). A 10 μl sample of the protein was injected into microbore HPLC, and the protein was eluted with a 0.5 × 50 mm PLRP-S column (8 μm particle diameter, 4000 Å pore size; Michrom BioResources, Auburn, CA) with mobile phase A (acetonitrile/water/acetic acid/trifluoroacetic acid, 2/98/0.1/0.02) and B (acetonitrile/water/acetic acid/trifluoroacetic acid, 90/10/0.09/0.02). The gradient used to elute protein was from 5% to 95% of mobile phase B in 10 min followed by 95% B for 5 min at a flow rate of 20 μl/min. Automated acquisition of full scan MS spectra was executed by Finnigan Excalibur™ software. The settings for the ESI were as follows: spray voltage, 4.5 kV; nitrogen sheath gas and auxiliary gas flow rates, 60 and 5 psi, respectively; capillary temperature, 200 °C; capillary voltage, 22 V; tube lens offset, 40 V. The electron multiplier was set at −860 V; the scan time setting was performed with 50 msec of max injection time for full scan. The target number of ions for MS was $1 \times 10^8$. The full scan range for MS was 300–2000 Da. The Finnigan-MAT BIOWORKS software to afford the MH+ m/z value(s) of the protein sample deconvoluted the acquired convoluted protein spectra from LCQ.

## RESULTS

### Kinetic mechanism of ERK2 in the reverse direction

To begin an investigation into the mechanism of product release we first examined the reaction in the reverse direction, which has the potential to provide a measure of the reversibility of the reaction as well as insight into the interactions of the product ADP and *p*-Ets while bound to ERK2. We have previously examined the kinetic mechanism of ERK2 in the forward direction by initial velocity measurements in both the absence and presence of products and shown it to be a random-order ternary-complex mechanism with the formation of two abortive complexes (Scheme 2). The reverse reaction was studied by following the phosphorylation of ADP, using $^{32}$P labeled *p*-Ets as the phosphate donor. *p*-Ets is readily prepared by incubating Ets with ATP in the presence of ERK2 (20). Initial velocity studies were performed using 50 nM ERK2, varied concentrations of ADP (100–5000 μM) and $^{32}$P-*p*-Ets (1.8–90 μM) under identical buffer conditions to those used to study the reaction in the forward direction (20) (e.g. 27 °C, 25 mM HEPES pH 7.4, 100 mM KCl, 2 mM DTT, 40 μg/mL BSA, and 20 mM $MgCl_2$). By applying aliquots of each reaction to thin layer chromatography plates and developing the plates in acidic 20% methanol the convenient monitoring of the formation of [γ–$^{32}$P]-ATP was possible over the course of the reaction. Quantification of reaction progress was then achieved by determining the $^{32}$P associated with the migrating ATP using a phosphorimager (see Experimental Procedures). The observed rate constants, $k_{obs}$, were generally reproducible to within 10%. The resulting experimental data was used to create plots

of $1/k_{obs}$ *versus* 1/[*ADP*] or 1/[*p*-Ets] (Figure 2A and B). In both cases reciprocal plots clearly intersect to the left of the ordinate and above the abscissa, consistent with a sequential mechanism (32). Analysis of the data according to eqn. 1 provided the kinetic parameters shown in Table 1. Several features of these parameters are notable. For example, the Michaelis constants for Ets and *p*-Ets ($K_m^{Ets}=18\quad\mu$M and $K_m^{p-Ets}=13\quad\mu$M) are similar suggesting that the phosphorylation of Ets has little effect on its ability to bind ERK2.

## Kinetic mechanism of *p*-Ets binding

To evaluate the mechanism of *p*-Ets binding, a fluorescent derivative called *p*-Ets-*F* was utilized, which contains a single fluorescein-labeled cysteine at residue 31 (21). To evaluate the binding of *p*-Ets-*F* to ERK2, we adopted a fluorescence anisotropy approach used previously to assess the binding of Ets to ERK2 (21). Assays were performed in 25 mM HEPES pH 7.5, 50 mM KCl, 20 mM $MgCl_2$, 40 μg/mL BSA, 0.1 mM EDTA, 0.1 mM EGTA, 1.3% glycerol, and 2 mM DTT containing ERK2 (0–20 μM) and 100 nM *p*-Ets-*F* in a final volume of 60 μl. Fluorescence anisotropy measurements were made at 27 °C using a Fluorolog Model FL3-11 fluorometer (Jobin Yvon, Edison, NJ). Thus, a 100 nM solution (final concentration) of *p*-Ets-*F* was added to varying concentrations of activated ERK2 and the resulting anisotropy determined (Figure 3B). As expected the anisotropy values increased upon the addition of ERK2, consistent with the formation of a *p*-Ets-*F*•ERK2 complex. As reported previously activated ERK2 is monomeric under the assay conditions (21), therefore the binding model shown in Scheme 3A is assumed. Upon fitting the data to equations 2 and 3,[7] a dissociation constant of $K_d^{p-Ets-F}=4.8\pm0.5\quad\mu$M was obtained for the binding of *p*-Ets-*F* to activated ERK2.

$$R=\frac{(I_v+2GI_H)_{bound}}{(I_v+2GI_H)_{free}} \qquad \text{(eqn. 2)}$$

$$r=\frac{\frac{\left(K_d^{p-Ets-F}+[S_t]+[E_t]\right)-\sqrt{\left(-K_d^{p-Ets-F}-[S_t]-[E_t]\right)^2-4[E_t][S_t]}}{2[S_t]}\left(r_bR-r_f\right)+r_f}{1+\frac{\left(K_d^{p-Ets-F}+[S_t]+[E_t]\right)-\sqrt{\left(-K_d^{p-Ets-F}-[S_t]-[E_t]\right)^2-4[E_t][S_t]}}{2[S_t]}(R-1)} \qquad \text{(eqn. 3)}$$

The binding affinity of *p*-Ets was then determined using a competition approach, according to Scheme 3A, previously used to determine the binding of Ets and PEA15 to ERK2 (21, 33). Thus, a solution containing a fixed concentration of *p*-Ets-*F* and active ERK2 was added to a solution containing varied concentrations of *p*-Ets. As expected, there is a decrease in the final anisotropy reading with increasing concentrations of *p*-Ets, indicating that *p*-Ets competes with *p*-Ets-*F* for binding to active ERK2 (Figure 3C). Simultaneous fitting of the data to the five equations describing the equilibria in Scheme 3A, eqns. 4–8, furnishes a single best fit for the dissociation constant of $K_d^{p-Ets}=7.3\pm0.5\quad\mu$M.

[7] *Parameters for fluorescence binding:* $r_f$ and $r_b$ are the anisotropies of the free and bound fluorescein-labeled protein, *R* is the ratio of fluorescent yields of the bound form and the free form of fluorescein-labeled protein S. $[S_t]$, $[B_t]$ and $[E_t]$ are the total concentration of *p*-Ets-*F*, *p*-Ets and ERK2. $[S_f]$, $[B_f]$ and $[E_f]$ are the concentrations of unbound forms of the *p*-Ets-*F*, *p*-Ets and ERK2. $I_V$ and $I_H$ are the intensity of the emission at polarizations both parallel and perpendicular to the excitation source and G is a factor to correct for instrumental differences in detecting emission components. Specifically, the G factor is the ratio of the intensity of the vertically and horizontally polarized emission components when the sample is excited with horizontally polarized light. Note *R* was determined to be 0.5 by measuring the fluorescence emission spectrum of *p*-Ets-*F* when bound to ERK2.

$$r = \frac{\frac{[ES]}{[S_t]}\left(r_b R - r_f\right) + r_f}{1 + \frac{[ES]}{[S_t]}(R-1)} \quad \text{(eqn. 4)}$$

$$[ES] = \frac{\left[E_f\right][S_t]}{K_{\mathrm{d}}^{p-\mathrm{Ets}-F} + \left[E_f\right]} \quad \text{(eqn. 5)}$$

$$K_{\mathrm{d}}^{p-\mathrm{Ets}} = \frac{\left[E_f\right]\left[B_f\right]}{[EB]} \quad \text{(eqn. 6)}$$

$$B_t = B_f + EB \quad \text{(eqn. 7)}$$

$$E_t = E_f + EB \quad \text{(eqn. 8)}$$

This anisotropy study suggested that *p*-Ets-*F* is a reasonable surrogate for assessing the interactions of *p*-Ets with ERK2, as the difference in the affinity of each protein for ERK2 is only 1.5-fold. During the course of the binding studies we determined that the fluorescence emission of *p*-Ets-*F* decreases significantly upon binding to ERK2 (Figure. 3A). Therefore, a stopped-flow analysis was conducted at 27 °C to examine the mechanism of binding.

To measure the rate of *p*-Ets-*F* binding to ERK2 an excitation wavelength of 492 nm was used. Figure 4 shows representative experiments where, in the presence of 20 mM $Mg^{2+}$, a solution of *p*-Ets-*F* (200 nM) was rapidly mixed with an equal volume of a solution containing either ERK2 (0–20 μM) alone (Figure 4A), or ERK2 (0–20 μM) and 8 mM ADP (Figure 4B). Each of the traces shown represent the average of five runs and were assessed in terms of several kinetic models, using the global fitting program KinTek Explorer Pro (25,26). In all cases the best fit to the data corresponded to the single-step binding model shown in Scheme 3B. In the absence of ADP the rate constants describing *p*-Ets-*F* binding are $k_{p\text{-}Ets\text{-}F}$ = 9.4 ± 0.3 × $10^6$ $M^{-1}s^{-1}$ and $k_{-p\text{-}Ets\text{-}F}$ = 121 ± 4 $s^{-1}$, which corresponds to a dissociation constant of $K_{\mathrm{d}}^{p-\mathrm{Ets}-F} = 13 \quad \mu\mathrm{M}$ (Figure 4A), which is in reasonable agreement with the value of $K_{\mathrm{d}}^{p-\mathrm{Ets}-F} = 4.8 \pm 0.5 \quad \mu\mathrm{M}$ determined by the anisotropy measurements in the presence of 1.3% glycerol. The presence of saturating ADP has only a marginal effect on these values (Table 2), providing further support for the notion that *p*-Ets and ADP do not interact energetically while bound to ERK2.

## Determining the Rate of ADP Release

To investigate the mechanism of ADP release from ERK2 we first determined its affinity by isothermal titration calorimetry. Figure 5 shows a typical titration where a change in the heat of the solution that accompanies the addition of MgADP to ERK2 (263 μM), signifies binding between the two molecules. Integration of the experimental isotherm using a single-site binding model established a dissociation constant of $K_{\mathrm{d}}^{\mathrm{ADP}} = 172 \pm 6 \quad \mu\mathrm{M}$ for ADP with a binding

stoichiometry of 1.02 ± 0.01 (Figure. 5). This value is in excellent agreement with the parameters determined from the analysis of the reaction in the reverse direction (Table 1).

In order to investigate the rate of ADP release from ERK2 a trapping experiment was performed, which allows measurement of individual points for a reaction time course on the millisecond to second timescale. The trapping approach has previously been used to estimate the rate of ATP and ADP release from protein kinase complexes (34–38). An assumption is that the rate of ADP release from the abortive complex, $E^{ADP}_{p-Ets}$, represents a good approximation of its rate of release from ERK2 during turnover. This appears to be a reasonable assumption, because as noted above there is little kinetic or thermodynamic evidence to suggest that the protein and nucleotide ligands interact significantly while bound to ERK2 (See Table 1). The approach depends on the ability to couple the rate of release of ADP from the $E^{ADP}_{p-Ets}$ abortive complex to a measurable signal. In the case of the experimental design shown in Scheme 4A, this signal is the formation of product (e.g. *p*-Ets).

As part of the `trapping' approach two experiments are performed. In the first experiment (control experiment), ADP is mixed at the same time as ATP and Ets. In the second experiment (pre-equilibrium experiment) ERK2 is pre-incubated with ADP before the addition of Ets and ATP.

**Control experiment—**Figure 6B depicts a typical time course for the formation of *p*-Ets obtained at 5 μM ERK2 (final) in the presence of 1 mM ADP and 5 mM ATP. In this experiment ERK2 was rapidly mixed with an equal volume of a second solution containing ATP (10 mM), ADP (2 mM) and Ets (300 μM) (open circles). After a designated period (2–150 ms), reactions were quenched with acid *via* a second mixing event. Labeled *p*-Ets was then recovered and quantified after calibration of the machine as described previously (24). This time course is characterized by an initial burst followed by a slower, linear phase which may be described by the kinetic model shown in Scheme 4B (24). According to this model the binding of ATP and Ets to ERK2 is assumed to be fast and irreversible under the conditions employed. Thus, the reaction rate is dependent on two irreversible steps: the rate of product formation on the enzyme, $k_p$, and the rate of product release from the enzyme, $k_{off}$. According to this model the observed rate of turnover is a function of the steady-state concentration of the ternary complex and is related to the slope of the linear phase of the reaction. Based on the $K^{ADP}_d$ of 172 μM for ADP and $K^{ATP}_i$ of 65 μM for ATP (20), it may be estimated that under steady-state conditions >90% of ERK2 will be complexed with ATP, with less than 10% in complex with ADP. Consistent with this estimation, a comparison with previous experiments performed in the absence of ADP (24), suggests that the ADP in the trapping experiment has little effect on the steady-state rate under the experimental conditions.

**Pre-equilibrium experiment—**After determining that 1 mM ADP has a minimal effect on the rate of ERK2 in the presence of 5 mM ATP we examined the effect of pre-incubating ADP (2 mM) with ERK2 (10 μM) before rapidly mixing with ATP (10 mM) and Ets (300 μM). Syringe A contains ERK2 (10 μM) and ADP (2 mM). Based on the $K^{ADP}_d$ of 172 μM established by the isothermal titration calorimetry experiment, 92% of ERK2 is expected to be complexed with ADP in syringe A. Syringe B contains both ATP (10 mM) and Ets (300 μM) whose rapid binding to ERK2 has been established previously: binding occurs with apparent association rates in excess of 400 $s^{-1}$ at concentrations of 150 μM Ets and 2 mM ATP (24). In contrast to a `burst phase' that precedes the linear phase in the control experiment an initial lag phase is observed, which precedes the linear steady-state phase. The data in Figure 6A were analyzed using KinTek Explorer Pro (25,26), according to Scheme 4A yielding the following rate

constants; $K^{a}_{-ADP}$=61 ± 13 $s^{-1}$, $k_p$ = 105 ± 30 $s^{-1}$ and $k_{off}$ = 85 ± 20 $s^{-1}$, which are in good agreement with previously determined values of $k_p$ = 106 ± 8 and $s^{-1}$ and $k_{off}$ = 59 ± 6 $s^{-1}$.

### Towards a structural understanding of catalysis: a model of the ERK2-Ets-1 interaction

**Modeling for ERK2-Ets 28–138 interactions—**To gain insight into how ERK2 binds Ets-1 we sought to predict how the SAM domain of Ets-1 and ERK2 might interact. To this end, a complex structure consisting of active ERK2 (PDB ID: 2ERK) and residues 28–138 of Ets-1 (PDB ID: 2JV3) was predicted using the molecular mechanics modeling approaches available in the software package TINKER (29), as described in Experimental Procedures. A feature of the predicted complex (Figure 7) is an interaction between loop-13 and the αG helix of ERK2 with the helix 4/loop/helix 5 locus of the SAM domain of Ets-1. The general features of the model appear to be quite robust as they were predicted using several different approaches (e.g. different starting points and constraints).

To provide experimental support for the model Lys-229 and His-230 of loop-13 were simultaneously mutated to Thr and Asp respectively, the corresponding residues in p38 MAPK, a MAPK that binds Ets-1 weakly.[8] The K229T/H230D mutant was expressed, purified and fully activated in the same manner as the wild type enzyme. Activation was confirmed by mass spectrometric analysis, which showed that ~ 2 mol/mol of phosphate was incorporated into the protein by MKK1G7b (a constitutively active form of MKK1) and that only one radio-labeled peptide of the correct mass (corresponding to residues 178–196) was observed following trypsinization of the activated protein (data not shown). When examined in a kinase assay the mutant displayed a 44-fold decrease in the specificity constant, $k_{cat}/K_m$, towards the Ets protein ($k_{cat}$ = 4.2 ± 0.5 $K_m$ = 82.0 ± 20), suggesting that this locus mediates an important interaction between ERK2 and Ets-1, in support of the predicted model. We consider it unlikely that the mutations in these residues cause a global structural change because the ATPase activity of the mutant is comparable to the wild type enzyme (data not shown).

## DISCUSSION

### Reverse kinetics

Previous transient kinetic studies showed that product release partially limits the rate of Ets turnover by ERK2 (24), however these studies did not identify which product dissociation step limits turnover. As *p*-Ets binds ERK2 some 20-fold more tightly than ADP (Table 1 and 2) it was of interest to examine whether this translated to a slower rate of product release. This question is pertinent, because ERK2 has a number of diverse substrates and so it is of interest to determine how ERK2 and its substrates have co-evolved to maximize the efficiency of substrate turnover. One prediction is that, given that ADP release is a common step regardless of which substrate is being phosphorylated by ERK2, then ADP release should at least be partially rate-limiting in cases where substrate turnover is efficient.

To investigate the process of product release we first decided to examine the reaction in the reverse direction. This has the potential to provide information on the nature of product interactions as well as the order of product binding. Based on a previous examination of the reaction in the forward direction we knew the reverse reaction must occur through a sequential mechanism (32) (Scheme 2). From the kinetic analysis of ATP formation shown in Figure 2 we determined that the magnitude of the catalytic constant for the reverse reaction,$k^{r}_{cat}$, is 0.2 $s^{-1}$. This value is significantly smaller than the anticipated rate constant for the release of either ATP or Ets (the products of the reverse reaction) (39), suggesting that steps associated with

[8]Unpublished observations

the interconversion of the ternary complexes, $k_{-p}$ and not ATP or Ets release are likely to be rate-limiting in the reverse direction. Furthermore, as the rate of binding of ADP and *p*-Ets is considerably faster than $k^{r}_{cat}$ the reaction must occur through a rapid-equilibrium mechanism in the reverse direction. Therefore, an ordered mechanism of ADP and *p*-Ets binding may be excluded on the basis that neither of the double reciprocal plots for the reverse reaction in Figure 2A and 2B intersect on the y-axis (32). The data are therefore consistent with a rapid-equilibrium random-order ternary-complex mechanism for the reaction in the reverse direction. Accordingly, upon fitting the data in Figure 2 to equation 1 kinetic parameters for the reaction (according to Scheme 2) were obtained (please see Table 1). These kinetic parameters suggest that, in the presence of 10 mM $Mg^{2+}$, little interaction occurs between ADP and *p*-Ets upon binding ERK2, with *p*-Ets binding some 20-fold more tightly than ADP.

$$K_{eq}=k^{f}_{cat}K^{ADP}_{d}K^{p-Ets}_{m}/k^{r}_{cat}K^{ATP}_{i}K^{Ets}_{m} \quad \text{(Eqn 9)}$$

By examining the reaction in the reverse direction we are able to use the Haldane relationship (equation 9) to estimate an equilibrium constant of $K_{eq}$ = 250 for the reaction in solution (Scheme 5). This value is smaller than $K_{eq}$ reported for the reaction between ATP and two peptides Ac-LRRASLG (40) and PLARTLSVAGLPGKK (41), suggesting that sequence and/or protein structure may influence the equilibria. Interestingly, the magnitude of the equilibrium for Thr-38 phosphorylation by ATP on ERK2 may be estimated by taking the ratio of the rate of phosphoryl transfer in the forward and reverse directions. In the forward direction, the rate constant of $k_{p}$ = 105 $s^{-1}$, was determined from single turnover experiments (24). In the reverse direction a rate constant of $k^{r}_{cat}$=0.2 $s^{-1}$ may be attributed to phosphoryl transfer, $k_{-p}$. These values predict an equilibrium of $K_{int}$ = 105/0.2 = 525 indicating that $K_{eq}$ and $K_{int}$ are almost identical (Scheme 5).

## Product release

We found that the fluorescent protein *p*-Ets-*F* binds ERK2 with similar affinity to the Ets protein (Figure 3A) and therefore we used it to assess the mechanism of *p*-Ets binding in transient kinetic experiments. Analysis of the kinetic transients shown in Figure 4 by global fitting suggests that *p*-Ets-*F* binds ERK2 through a single-step mechanism with rate constants of $k_{p\text{-}Ets\text{-}F}$ = 9.4 ± 0.3 × $10^{6}$ $M^{-1}s^{-1}$ and $k_{-p\text{-}Ets\text{-}F}$ = 121 ± 3.8 $s^{-}$ for association and dissociation respectively. Similar results were obtained when ERK2 was pre-incubated with a saturating concentration of ADP (Table 2). Interestingly, the rate constant for *p*-Ets-*F* dissociation, $k_{-p\text{-}Ets\text{-}F}$, is approximately twice the magnitude of $k_{off}$, suggesting that Ets has indeed evolved to facilitate rapid dissociation. While we consider $k_{-p\text{-}Ets\text{-}F}$ to be a reasonable approximation to $k_{p\text{-}Ets}$ as both *p*-Ets-*F* and *p*-Ets bind ERK2 with similar affinities (Table 2) the possibility that the rates of dissociation may be significantly different cannot be excluded. The similarity in the kinetic mechanism and magnitude of the parameters for the binding of *p*-Ets-*F* to ERK2 and the ERK2•ADP binary complex support the contention that Ets does not significantly interact with ADP upon binding. This also argues against a mechanism where a rate-limiting conformational change precedes the release of the products, because such a step should be apparent upon the binding of *p*-Ets-*F* to the binary complex.

To assess the rate of ADP release from ERK2 we turned to a trapping technique used previously to examine the release of ADP from other protein kinases (34–37). This technique relies on the ability of excess ATP and substrate to trap the enzyme as a productive ternary complex following rapid mixing with the enzyme, which had been pre-equilibrated with ADP and provides a value for $k^{a}_{\text{-ADP}}$ (Scheme 4A). Figure 6A shows an experiment where ADP was either pre-incubated with ERK2 or added at the same time as ATP. A comparison of

experiments A and B show clearly that pre-incubation with ADP abolishes the burst phase and introduces a lag phase without altering the magnitude of the steady-state linear phase. A global fit of the data to the mechanisms in Schemes 5A and B using numerical integration provided a good minimized fit and rate constants of $k^a_{\text{-ADP}} = 61 \pm 13\ s^{-1}$, $k_p = 105 \pm 30\ s^{-1}$ and $k_{off} = 85 \pm 20\ s^{-1}$.

Taken together these data support the notion that the Ets protein has evolved to interact in such a manner with ERK2 that both its phosphorylation and dissociation are comparable in rate to ADP dissociation. Recently, an iso random bi bi mechanism was proposed for the phosphorylation of Ets by ERK2 (42) to account for the observed effects of adding viscosogens to the steady-state reaction. According to the mechanism an isomerization step is partially rate-limiting, however, this would appear to be inconsistent with the observed kinetic data. For example, the iso random bi bi mechanism predicts a lag in the formation of *p*-Ets under single turnover conditions, which is clearly not the case in Figure 6B, (dotted line). While we cannot explain the reason for the discrepancy, we note however that the effect of viscosogens on the properties of proteins is often very difficult to predict.

## Recognition of Ets-1by ERK2

It is of interest to understand how Ets binds ERK2 in order to facilitate the efficient and specific phosphorylation of Thr-38. Enzymes have evolved under selective pressure to facilitate cellular processes and ERK2 has the formidable task of phosphorylating a specific subset of cellular proteins (perhaps as many as 100) with a relatively high specificity constant (typically ~ $10^6$ $M^{-1}s^{-1}$). Thus, an important broader goal is to determine distinguishing features of ERK2-substrate interactions. To address these issues and to provide a possible structural basis for the mechanism of Ets-1 phosphorylation we examined the complex formed between activated ERK2 and residues 28–138 of Ets-1 (Figure 7).

To build the model we began with a recent structure of CDK2/cyclin A3 bound to the optimal peptide substrate HHASPRK, which reveals how CDK2/cyclin A3 binds the P+1 proline (43). Like ERK2 CDK2 is a proline-directed protein kinase. A characteristic feature of the P +1 pocket of CDK2 is the unusual left-handed conformation of Val-164 ($\Phi$=72.5° and $\psi$=130.8°), whose backbone carbonyl is oriented away from the opening of the pocket towards an arginine that is exclusively conserved in proline-directed kinases (Arg-169 in CDK2). Given the similarity in the conformation of the activation segments of ERK2 and CDK2, these enzymes are expected to bind the P+1 proline in a similar manner. Therefore, the model was built by fixing Thr-38 and Pro-39 of Ets-1 at the active site of ERK2 according to the CDK2/peptide structure, before allowing the structure to relax.

The modeling predicts an interaction between helix 4/loop/helix 5 in the SAM domain of Ets-1 and the loop 13/αG helix motif of ERK2 (Figure 7). This predicted interaction is consistent with previous mutagenesis studies on Ets-1 where residues Leu-114 and Phe-120, which lie in the loop between H4 and H5 were shown to compromise the ability of ERK2 to phosphorylate Ets-1 both *in vitro* and in cells (17). Furthermore, several years ago, hypothesizing that MAPKs are related through gene duplication, Caffrey et al. performed a computational analysis to predict regions of functional difference between subfamilies of MAPKs (44). They reasoned that after gene duplication, a region of a protein that confers a functional difference between subfamilies, such as specificity, undergoes a physicochemical change and then conserves this change amongst the subfamily. When they compared the primary sequences of the MAPKs and searched for regions amongst subfamily members that significantly changed after gene duplication, but remained conserved amongst subfamily members thereafter they identified five regions of interest.[9] One region corresponded to residues Lys-229 and His-230, which lie at the end of loop-13 of ERK2. These residues appear to be important for the recognition of a number of ligands to ERK2 including MAPKK1 (45), phosphoprotein enriched in

astrocytes-15 kDa (PEA-15) (46), MAPK phosphatase 3 (MKP3), and Elk-1 (47). When we tested the ability of the K229T/H230D mutant to phosphorylate Ets it exhibited a 44-fold decrease in $k_{cat}/K_m$ compared to wild type ERK2 lending support to our model.

### Mechanism

A feature of our model is that compared to unbound Ets-1, helix 1 (H1) of the SAM domain unwinds significantly to accommodate the binding of the Thr-38/Pro-39 motif in the active site. This is interesting, because our studies have suggested that the binding of the Thr/Pro motif in the active site of ERK2 may not be a feature of the ground-state ternary complex, but rather a feature of an intermediate along the reaction pathway (21,23). It is possible, for example, that the unfavorable cost of unwinding H1 could offset the favorable energy associated with the appropriate Thr-Pro binding to ERK2. While the model does not address how the *N*-terminus of Ets-1 (residues 1–27) binds to ERK2, experimental evidence suggests that it may interact within the DRS of ERK2 (21,22).

Based on the current and previous data (21,22) we propose a kinetic mechanism for the phosphorylation of Ets-1 where, following docking, Thr-38 becomes localized within the proximity of the ERK2 active site in a ground-state ternary complex, $^{inact}E_{Ets}^{ATP}$ (Scheme 6). Two discrete docking sites found in the SAM domain and the *N*-terminus of Ets-1 span Thr-38 and stabilize this complex through interactions with the MAPK insert and the DRS, respectively. Accordingly, the ground state complex then rearranges ($K_2$) to place the Thr-Pro motif in the active site primed for phosphorylation to give $^{act}E_{Ets}^{ATP}$. All steps following the formation of the ground state ternary complex up to and including the phosphoryl transfer step correspond to $k_p$ in Scheme 1, while all steps after the phosphorylation step contribute to $k_{off}$. Other features of the mechanism are that the dissociation of *p*-Ets from ERK2 is at least as fast as the dissociation of ADP and that products can dissociate in any order.

## Acknowledgments

This research was supported in part by the grants from the Welch Foundation (F-1390) to KND and the National Institutes of Health to KND (GM59802) and to PR (GM79686).

## REFERENCES

1. Duesbery NS, Webb CP, Vande Woude GF. MEK wars, a new front in the battle against cancer. Nat Med 1999;5:736–737. [PubMed: 10395314]
2. Kohno M, Pouyssegur J. Targeting the ERK signaling pathway in cancer therapy. Ann Med 2006;38:200–211. [PubMed: 16720434]
3. Kohno M, Pouyssegur J. Pharmacological inhibitors of the ERK signaling pathway: application as anticancer drugs. Prog Cell Cycle Res 2003;5:219–224. [PubMed: 14593716]
4. Milella M, Kornblau SM, Andreeff M. The mitogen-activated protein kinase signaling module as a therapeutic target in hematologic malignancies. Rev Clin Exp Hematol 2003;7:160–190. [PubMed: 14763161]
5. Sebolt-Leopold JS. Development of anticancer drugs targeting the MAP kinase pathway. Oncogene 2000;19:6594–6599. [PubMed: 11426644]
6. Weinberg, RA. The biology of Cancer. 2006.
7. Sivaraman VS, Wang H, Nuovo GJ, Malbon CC. Hyperexpression of mitogen-activated protein kinase in human breast cancer. J Clin Invest 1997;99:1478–1483. [PubMed: 9119990]

[9]A computational study was carried out by Caffrey *et al.* to predict regions of MAPKs conferring specificity differences amongst the MAPK subfamily members (41) Residues identified in this study fall into five loci on the surface of ERK2: (#1: His-59, Tyr-62, Gln-64, Leu-67), (#2: Tyr-111, Lys-112, Cys-125, Leu-154, Thr-157, Thr-158), (#3:Glu-184), (#4: Lys-201, Gly-202, Lys-205, and Ser-206), and (#5: Lys-229, His-230).

8. Bos JL. ras oncogenes in human cancer: a review. Cancer Res 1989;49:4682–4689. [PubMed: 2547513]
9. Solit DB, Garraway LA, Pratilas CA, Sawai A, Getz G, Basso A, Ye Q, Lobo JM, She Y, Osman I, Golub TR, Sebolt-Leopold J, Sellers WR, Rosen N. BRAF mutation predicts sensitivity to MEK inhibition. Nature 2006;439:358–362. [PubMed: 16273091]
10. Thottassery JV, Sun Y, Westbrook L, Rentz SS, Manuvakhova M, Qu Z, Samuel S, Upshaw R, Cunningham A, Kern FG. Prolonged extracellular signal-regulated kinase 1/2 activation during fibroblast growth factor 1- or heregulin beta1-induced antiestrogen-resistant growth of breast cancer cells is resistant to mitogen-activated protein/extracellular regulated kinase kinase inhibitors. Cancer Res 2004;64:4637–4647. [PubMed: 15231676]
11. Marampon F, Ciccarelli C, Zani BM. Down-regulation of c-Myc following MEK/ERK inhibition halts the expression of malignant phenotype in rhabdomyosarcoma and in non muscle-derived human tumors. Mol Cancer 2006;5:31. [PubMed: 16899113]
12. Gysin S, Lee SH, Dean NM, McMahon M. Pharmacologic inhibition of RAF-->MEK-->ERK signaling elicits pancreatic cancer cell cycle arrest through induced expression of p27Kip1. Cancer Res 2005;65:4870–4880. [PubMed: 15930308]
13. Brown JR, Nigh E, Lee RJ, Ye H, Thompson MA, Saudou F, Pestell RG, Greenberg ME. Fos family members induce cell cycle entry by activating cyclin D1. Mol Cell Biol 1998;18:5609–5619. [PubMed: 9710644]
14. Eferl R, Wagner EF. AP-1: a double-edged sword in tumorigenesis. Nat Rev Cancer 2003;3:859–868. [PubMed: 14668816]
15. Davies H, Bignell GR, Cox C, Stephens P, Edkins S, Clegg S, Teague J, Woffendin H, Garnett MJ, Bottomley W, Davis N, Dicks E, Ewing R, Floyd Y, Gray K, Hall S, Hawes R, Hughes J, Kosmidou V, Menzies A, Mould C, Parker A, Stevens C, Watt S, Hooper S, Wilson R, Jayatilake H, Gusterson BA, Cooper C, Shipley J, Hargrave D, Pritchard-Jones K, Maitland N, Chenevix-Trench G, Riggins GJ, Bigner DD, Palmieri G, Cossu A, Flanagan A, Nicholson A, Ho JW, Leung SY, Yuen ST, Weber BL, Seigler HF, Darrow TL, Paterson H, Marais R, Marshall CJ, Wooster R, Stratton MR, Futreal PA. Mutations of the BRAF gene in human cancer. Nature 2002;417:949–954. [PubMed: 12068308]
16. Biondi RM, Nebreda AR. Signalling specificity of Ser/Thr protein kinases through docking-site-mediated interactions. Biochem J 2003;372:1–13. [PubMed: 12600273]
17. Seidel JJ, Graves BJ. An ERK2 docking site in the Pointed domain distinguishes a subset of ETS transcription factors. Genes Dev 2002;16:127–137. [PubMed: 11782450]
18. Qiao F, Bowie JU. The many faces of SAM. Sci STKE2005. 2005 re7.
19. Waas WF, Dalby KN. Purification of a model substrate for transcription factor phosphorylation by ERK2. Protein Expr Purif 2001;23:191–197. [PubMed: 11570862]
20. Waas WF, Dalby KN. Transient protein-protein interactions and a random-ordered kinetic mechanism for the phosphorylation of a transcription factor by extracellular-regulated protein kinase 2. J Biol Chem 2002;277:12532–12540. [PubMed: 11812784]
21. Callaway KA, Rainey MA, Riggs AF, Abramczyk O, Dalby KN. Properties and regulation of a transiently assembled ERK2.Ets-1 signaling complex. Biochemistry 2006;45:13719–13733. [PubMed: 17105191]
22. Abramczyk O, Rainey MA, Barnes R, Martin L, Dalby KN. Expanding the Repertoire of an ERK2 Recruitment Site: Cysteine Footprinting Identifies the D-Recruitment Site as a Mediator of Ets-1 Binding. Biochemistry 2007;46:9174–9186. [PubMed: 17658891]
23. Rainey MA, Callaway K, Barnes R, Wilson B, Dalby KN. Proximity-induced catalysis by the protein kinase ERK2. J Am Chem Soc 2005;127:10494–10495. [PubMed: 16045329]
24. Waas WF, Rainey MA, Szafranska AE, Dalby KN. Two rate-limiting steps in the kinetic mechanism of the serine/threonine specific protein kinase ERK2: a case of fast phosphorylation followed by fast product release. Biochemistry 2003;42:12273–12286. [PubMed: 14567689]
25. Johnson KA, Simpson ZB, Blom T. Global kinetic explorer: a new computer program for dynamic simulation and fitting of kinetic data. Anal Biochem 2009;387:20–29. [PubMed: 19154726]
26. Johnson KA, Simpson ZB, Blom T. FitSpace explorer: an algorithm to evaluate multidimensional parameter space in fitting kinetic data. Anal Biochem 2009;387:30–41. [PubMed: 19168024]
27. Johnson, KA. The Enzymes. 3rd ed.. New York: 1992. Transient State Kinetic Analysis of Enzyme Reaction Pathways; p. 1-61.

28. Peterman BF. Measurement of the dead time of a fluorescence stopped-flow instrument. Anal Biochem 1979;93:442–444. [PubMed: 464271]
29. Ponder, JW. TINKER: Software Tools for Molecular Design. Washington University Medical School; 2006. http://dasher.wustl.edu/tinker/
30. Jorgensen WL, Maxwell DS, TiradoRives J. Development and testing of the OPLS all-atom force field on conformational energetics and properties of organic liquids. J Am Chem Soc 1996;118:11225–11236.
31. Pappu RV, Marshall GR, Ponder JW. A potential smoothing algorithm accurately predicts transmembrane helix packing (vol 6, pg 50, 1999). Nature Structural Biology 1999;6:199–199.
32. Segel, IH. Enzyme Kinetics: Behavior and Analysis of Rapid Equilibrium and Steady-State Enzyme Systems. Wiley Classics Library Edition ed., John Wiley & Sons, Inc.; 1993.
33. Callaway K, Abramczyk O, Martin L, Dalby KN. The anti-apoptotic protein PEA-15 is a tight binding inhibitor of ERK1 and ERK2, which blocks docking interactions at the D-recruitment site. Biochemistry 2007;46:9187–9198. [PubMed: 17658892]
34. Keshwani MM, Harris TK. Kinetic mechanism of fully activated S6K1 protein kinase. J Biol Chem 2008;283:11972–11980. [PubMed: 18326039]
35. Lieser SA, Shindler C, Aubol BE, Lee S, Sun G, Adams JA. Phosphoryl transfer step in the C-terminal Src kinase controls Src recognition. J Biol Chem 2005;280:7769–7776. [PubMed: 15623523]
36. Shaffer J, Sun G, Adams JA. Nucleotide release and associated conformational changes regulate function in the COOH-terminal Src kinase, Csk. Biochemistry 2001;40:11149–11155. [PubMed: 11551213]
37. Shaffer J, Adams JA. Detection of conformational changes along the kinetic pathway of protein kinase A using a catalytic trapping technique. Biochemistry 1999;38:12072–12079. [PubMed: 10508411]
38. Kong CT, Cook PF. Isotope partitioning in the adenosine 3',5'-monophosphate dependent protein kinase reaction indicates a steady-state random kinetic mechanism. Biochemistry 1988;27:4795–4799. [PubMed: 3048391]
39. Prowse CN, Hagopian JC, Cobb MH, Ahn NG, Lew J. Catalytic reaction pathway for the mitogen-activated protein kinase ERK2. Biochemistry 2000;39:6258–6266. [PubMed: 10821702]
40. Qamar R, Yoon MY, Cook PF. Kinetic mechanism of the adenosine 3',5'-monophosphate dependent protein kinase catalytic subunit in the direction of magnesium adenosine 5'-diphosphate phosphorylation. Biochemistry 1992;31:9986–9992. [PubMed: 1327136]
41. Kwiatkowski AP, Huang CY, King MM. Kinetic mechanism of the type II calmodulin-dependent protein kinase: studies of the forward and reverse reactions and observation of apparent rapid-equilibrium ordered binding. Biochemistry 1990;29:153–159. [PubMed: 2157478]
42. Wang ZX, Wu JW. The complete pathway for ERK2-catalyzed reaction. Evidence for an iso random Bi Bi mechanism. J Biol Chem 2007;282:27678–27684. [PubMed: 17652083]
43. Brown NR, Noble ME, Endicott JA, Johnson LN. The structural basis for specificity of substrate and recruitment peptides for cyclin-dependent kinases. Nat Cell Biol 1999;1:438–443. [PubMed: 10559988]
44. Caffrey DR, O'Neill LA, Shields DC. A method to predict residues conferring functional differences between related proteins: application to MAP kinase pathways. Protein Sci 2000;9:655–670. [PubMed: 10794408]
45. Robinson FL, Whitehurst AW, Raman M, Cobb MH. Identification of novel point mutations in ERK2 that selectively disrupt binding to MEK1. J Biol Chem 2002;277:14844–14852. [PubMed: 11823456]
46. Chou FL, Hill JM, Hsieh JC, Pouyssegur J, Brunet A, Glading A, Uberall F, Ramos JW, Werner MH, Ginsberg MH. PEA-15 binding to ERK1/2 MAPKs is required for its modulation of integrin activation. J Biol Chem 2003;278:52587–52597. [PubMed: 14506247]
47. Zhang J, Zhou B, Zheng CF, Zhang ZY. A bipartite mechanism for ERK2 recognition by its cognate regulators and substrates. J Biol Chem 2003;278:29901–29912. [PubMed: 12754209]

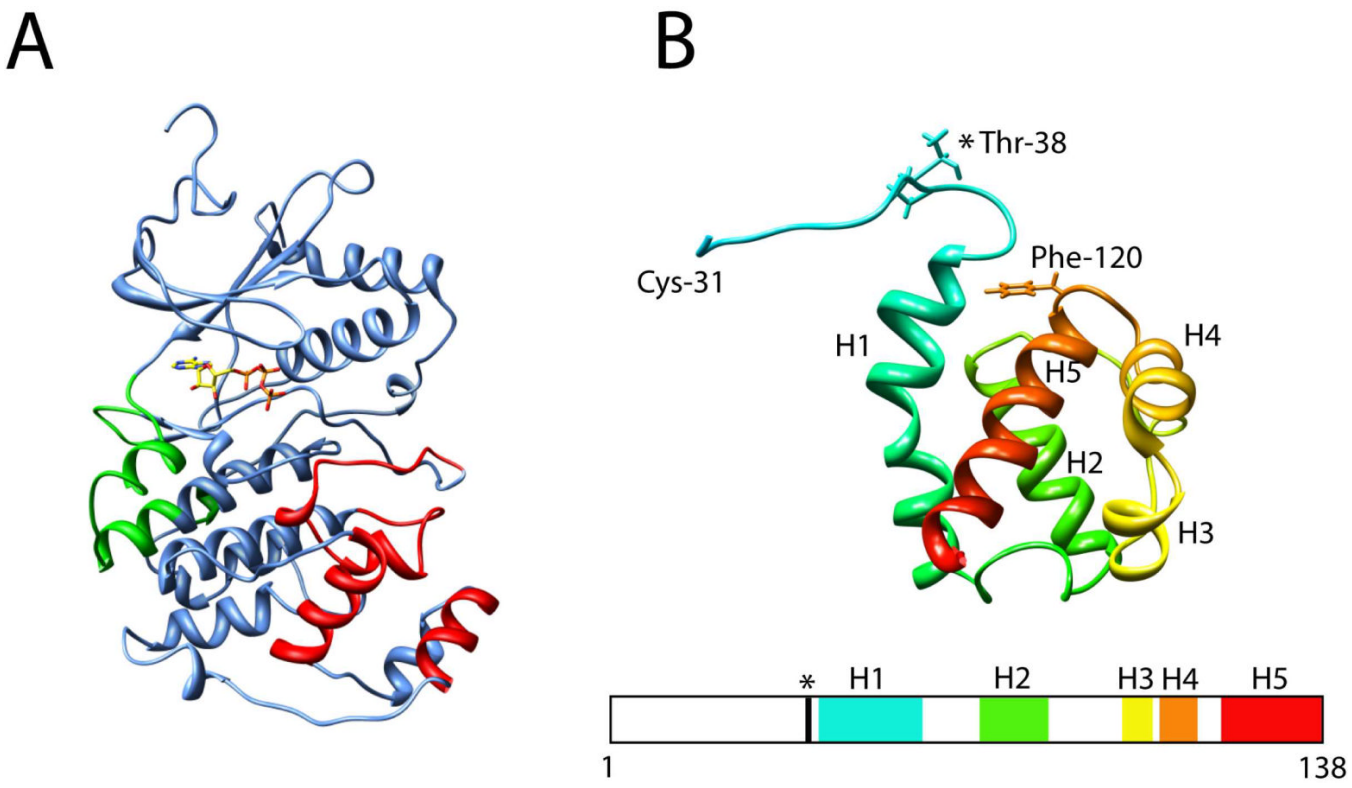


**Figure 1.**

A) Ribbon representation showing the structural features of MKK1–activated ERK2. *D-recruitment site (colored green)*—comprised of the reverse turn (Asn-156—Asp-160) between the β7 sheets and the β8 sheet, part of loop 7 (Glu-107—Asp-109), the αD helix (Leu-110—Thr-116), loop 8 (Gln-117—Ser-120) and part of the αE helix (Asn-121—Phe-127) and the *Common Docking domain* (Asp-316 and Asp-319). *F-recruitment site (colored red)*—this pocket shows a preference for aromatic residues at P+6 and P+8. The pocket is comprised of the *C*-terminus of the activation segment starting at Phe-181 through to the end of loop 12 (Phe-181–Thr-204), the αG helix (Tyr-231—Leu-242), and the α2L14 of the MAPK insert helix (Leu-256—Leu-263). The structure corresponds to PDB 2ERK. The ATP molecule is superimposed on the structure following alignment with PKA in PDB 1ATP. B) **Ribbon representation of residues 31–138 of Ets-1 (PDB 2JV3).** The ERK2 phosphorylation site, Thr-38, is shown as well as Phe-120 a residue implicated in ERK2 binding. The five Helices, H1-H5, that comprise the SAM domain of Ets-1 are shown.

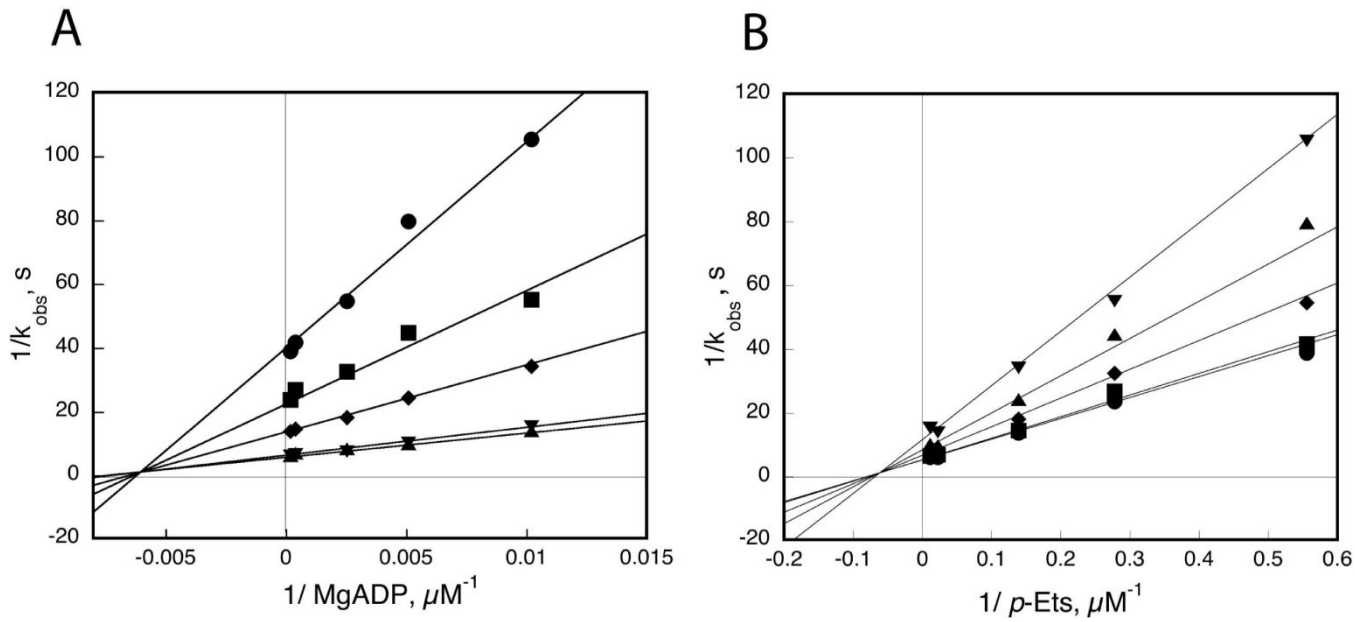


**Figure 2. Reverse Reaction Initial Velocity Studies**

Reactions were performed at 27 °C in kinase assay buffer (25 mM HEPES, pH 7.4, 2 mM DTT, 40 μg/mL BSA, and 20 mM $MgCl_2$). The ionic strength was maintained at 150 mM with KCl. Initial velocities were measured using ERK2 (50 nM), *p*-Ets (1.8–90 μM), and ADP (0.1–5 mM). The data were fitted to eqn. 1 and used to create reciprocal plots for **(A)** ADP at varied fixed concentrations of *p*-Ets (1.8 μM ●, 3.6 μM ■, 7.2 μM ◆, 45 μM ▼, and 90 μM ▲) and **(B)** *p*-Ets at varied fixed concentrations of ADP (100 μM ▼, 200 μM ▲, 400 μM ◆, 2.5 mM ■, and 5 mM ●). The parameters are presented in Table 1.

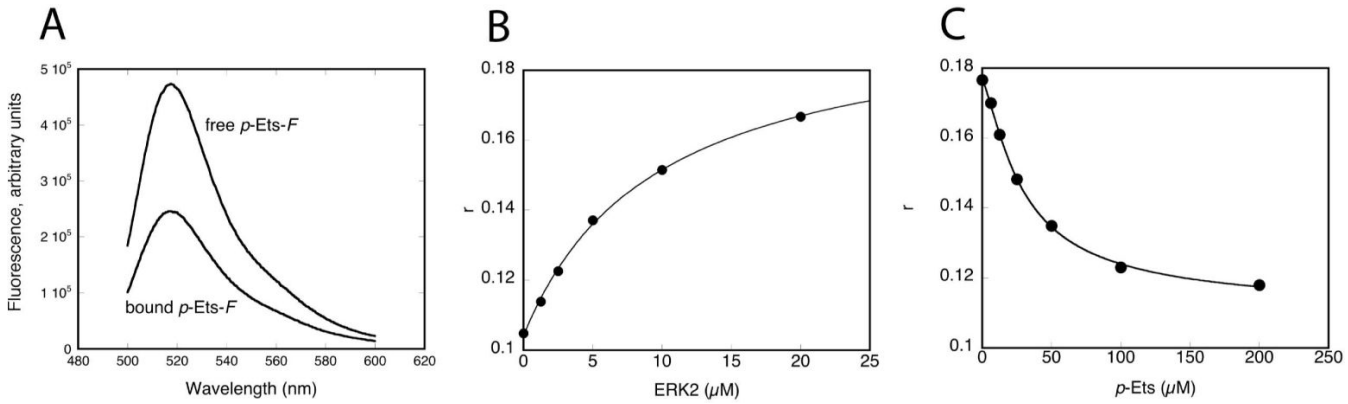


**Figure 3. Binding of *p*-Ets-*F***

Binding assays were performed in 25 mM HEPES pH 7.5, 50 mM KCl, 40 μg/mL BSA, 0.1 mM EDTA, 0.1 mM EGTA, 1.3% glycerol, and 2 mM DTT. **A.** The fluorescence emission spectrum of 100 nM *p*-Ets-*F* was examined in the absence and presence of 20 μM active ERK2. The sample was excited with light at 492 nm and an emission scan was performed from 500–600 nm. **B.** Binding of 100 nM *p*-Ets-*F* to active ERK2 (0–20 μM). Anisotropy values were averaged and the dissociation constants were determined by fitting the average anisotropy values to eqn. 3, according to Scheme 3A using Kaleidagraph 4.0 (Synergy software), where an *R* value of 0.5 was used. The best fit through the data furnished a value of $K_{\mathrm{d}}^{p-\mathrm{Ets}-F}=4.8\pm0.5\quad\mu\mathrm{M}$. **C.** A fluorescence anisotropy competition assay was performed with 100 nM *p*-Ets-*F*, 10 μM active ERK2, and varied *p*-Ets (0–200 μM). The experimental data was simultaneously fitted to equations 4–8 using an *R* value of 0.5 to give a value of $K_{\mathrm{d}}^{p-\mathrm{Ets}}=7.3\pm0.5\quad\mu\mathrm{M}$.

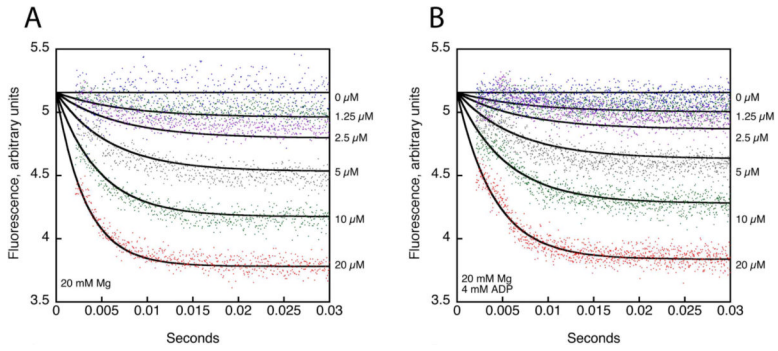


**Figure 4. Fluorescence Stopped-Flow Analysis of *p*-Ets-*F* Binding to Active ERK2**

**A. In the Absence of ADP**. Stopped flow experiments were conducted at 27 °C in 25 mM HEPES pH 7.5, 50 mM KCl, 2 mM DTT, 40μg/mL BSA, 0.1 mM EDTA, and 0.1 mM EGTA on a Kintek SF 2001 Airforce 1 stopped-flow apparatus fitted with 530 nm bandpass filters with a 25 nm bandwidth (Corion). An excitation wavelength of 492 nm was used. Syringe A was loaded with 200 nM solution of *p*-Ets-*F*. Syringe B was loaded with activated ERK2 (0–40 μM). The solutions were incubated at 27 °C for 3 minutes before being mixed to give a final concentration of 100 nM *p*-Ets-*F* and 0–20 μM ERK2. The reaction was monitored for a total of 30 msec and an average of 4–5 traces was used for data analysis. Data were fitted by numerical integration to the single step binding model in Scheme 3B using the program KinTek Explorer Pro (25, 26) to give $k_{+p\text{–Ets–}F} = 9.4 \pm 0.3 \times 10^6\ \mathrm{M^{-}s^{-}}$ and $k_{-p\text{–Ets–}F} = 121 \pm 3.8\ \mathrm{s^{-}}$.

**B. In the Presence of ADP**. The experiment was performed as in A except syringe B was also loaded with 8 mM ADP, to give a final concentration after mixing of 4 mM ADP. Data were fitted by numerical integration to the model in Scheme 3B using the program KinTek Explorer Pro (25, 26) to give $k'_{+p\text{–Ets–}F} = 6.2 \pm 0.2 \times 10^6\ \mathrm{M^{-1}s^{-1}}$ and $k'_{-p\text{–Ets–}F} = 123 \pm 3\ \mathrm{s^{-}}$.

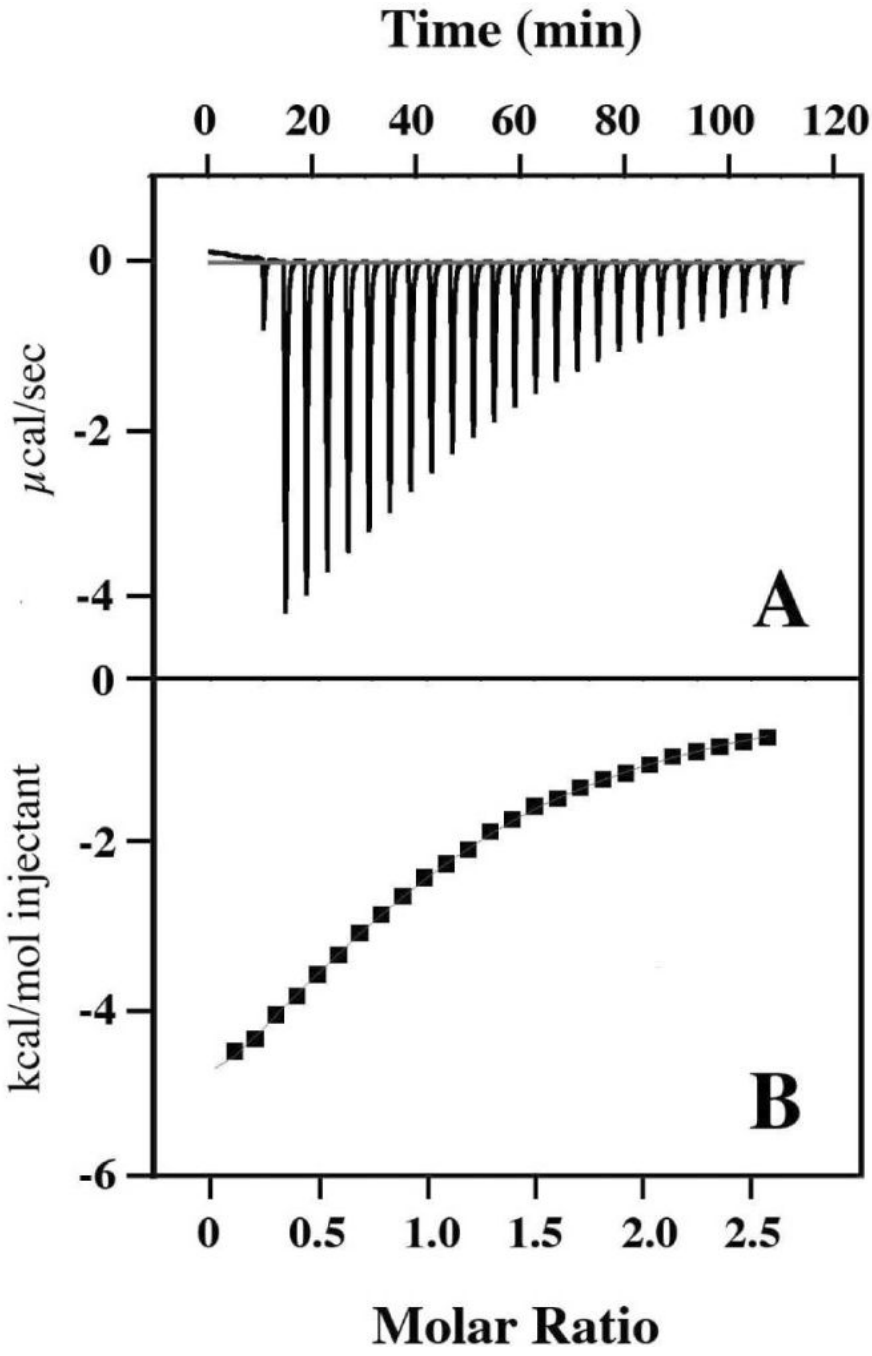


**Figure 5. Isothermal Titration Calorimetric Analysis of ADP Binding to Active ERK2**

Titrations were carried out on a MCS titration calorimeter (Microcal, Inc.) at 27 °C in 25 mM HEPES pH 8.0, 100 mM KCl, 2 mM β-mercaptoethanol, and 20 mM $MgCl_2$. **A**. *Top panel*—titration of MgADP (25 × 10 μL) into activated ERK2 (263 μM) at 27° C. The concentration of the MgADP solution was such that a 2.5 molar ratio of MgADP to active ERK2 would be reached in the cell upon the last injection; **B.** *Bottom panel*—integrated enthalpy change for each injection.

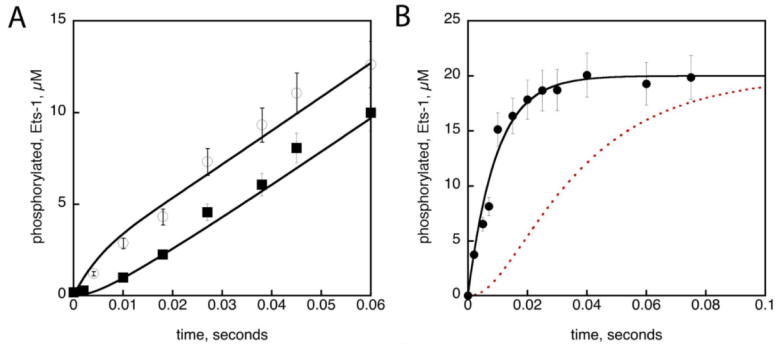


**Figure 6.**

**A. Burst Experiments in the presence of ADP.** Rapid Quench-flow experiments were conducted at 27 °C and pH 7.5 in buffer A (25 mM HEPES, 50 mM KCl, 2 mM DTT, 0.1 mM EDTA and 0.1 mM EGTA) containing 20 mM $MgCl_2$. Sample loop A was loaded with [$\gamma$-$^{32}$P]ATP (100–1000 c.p.m. pmol$^{-1}$) and ADP (0 mM closed squares; 2 mM open circles) while sample loop B was loaded with Ets, ERK2, and ADP (2 mM closed squares; 0 mM open circles). Final concentrations were MgATP (5 mM), MgADP (1 mM), Ets (150 μM), and ERK2 (5 μM). At set times reactions were quenched by the addition of 2 M $H_3PO_4$ and product formation was quantified as described in Experimental Procedures. The lines through the data correspond to the best fit by numerical integration to Schemes 4A and 4B ($k^a_{ADP}$ = 61 ± 13 s$^{-1}$, $k_p$ = 105 ± 30 s$^{-1}$ and $k_{off}$ = 85 ± 20 s$^{-1}$). **B. Single Turnover**. Rapid Quench-flow experiments were conducted at 27 °C and pH 7.5 in buffer A (25 mM HEPES, 50 mM KCl, 2 mM DTT, 0.1 mM EDTA and 0.1 mM EGTA) containing 20 mM $MgCl_2$. Sample loop A was loaded with [$\gamma$-$^{32}$P]ATP (100–1000 c.p.m. pmol$^{-1}$) while sample loop B was loaded with Ets, and ERK2. Final concentrations were MgATP (5 mM), Ets (20 μM), and ERK2 (136 μM) (solid circles). The line through the data correspond to the best fit by numerical integration to Scheme 1, where $k_p$ = 106 ± 8 s$^{-1}$. The dashed line corresponds to the predicted formation of product following rapid mixing, according to the iso random Bi Bi Mechanism and parameters reported by Wang et al. (42).

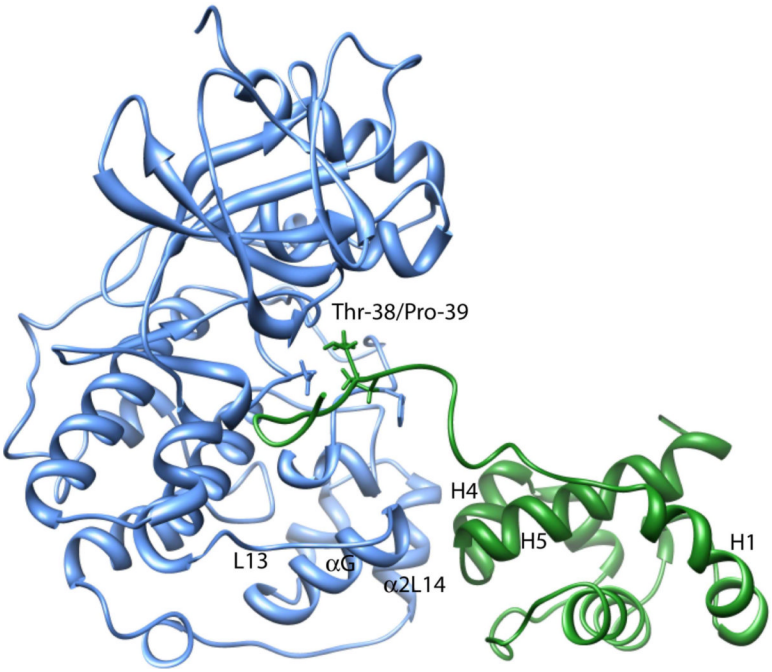


**Figure 7. Modeling for ERK2-Ets 28-138 interactions**

The complex structure of active ERK2 (PDB ID: 2ERK) and Ets (PDB ID: 2JV3) was predicted as described in Experimental Procedures.

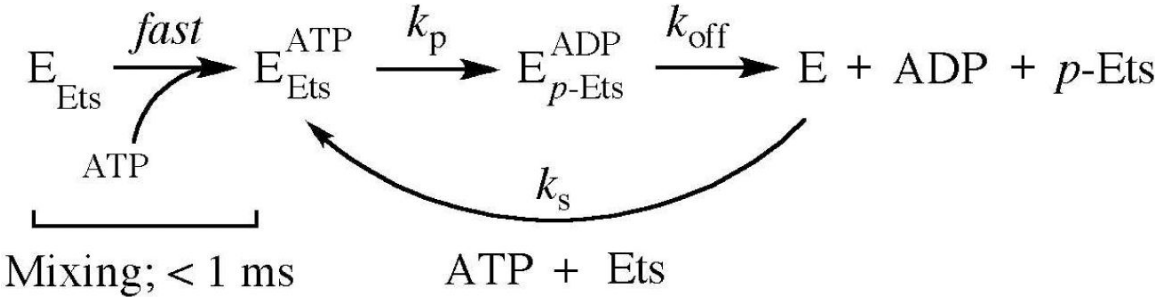


**Scheme 1.**

In rapid quench experiments, ERK2 and Ets are pre-incubated in standard assay buffer to form the binary complex $E_{Ets}$, before being rapidly mixed with ATP to form the ternary complex, $E^{ATP}_{Ets}$. This complex undergoes phosphorylation, $k_p$, followed by product release, $k_{off}$. In the presence of excess substrates, the conversion of free E to the ternary substrate complex, $k_s$, is assumed rapid.

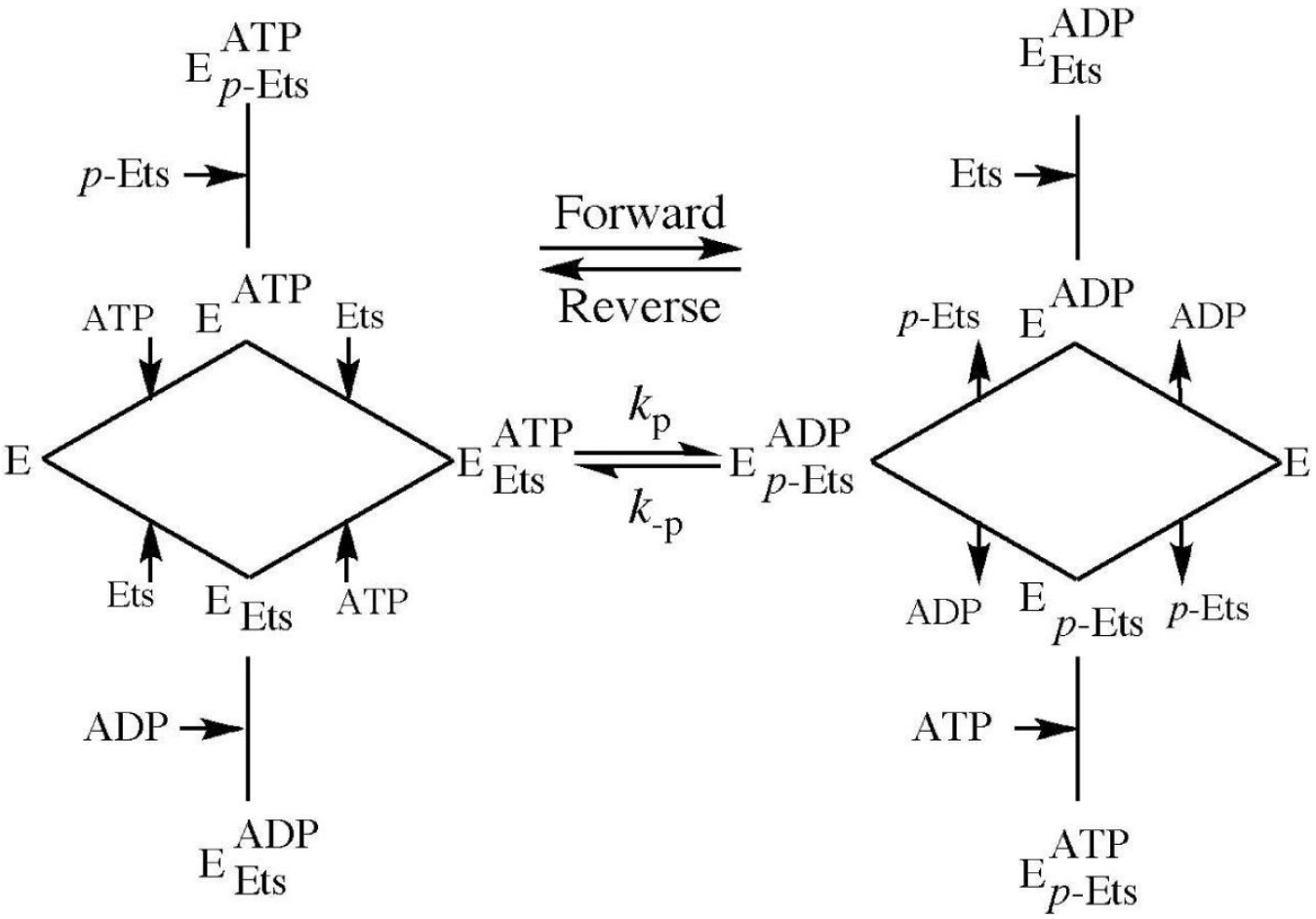


**Scheme 2.**
Random-order ternary complex mechanism involving two abortive complexes in the forward and reverse direction.

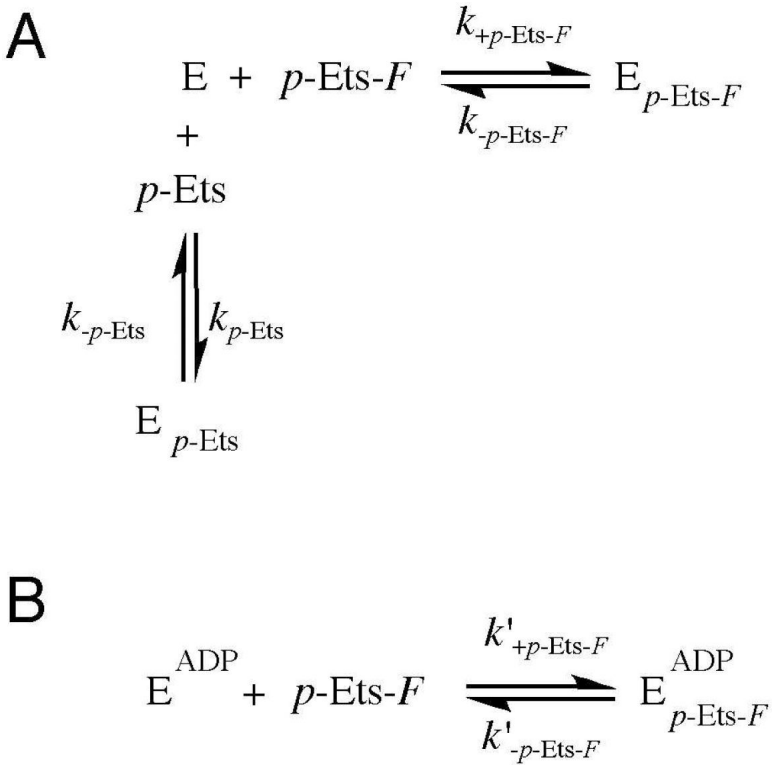


**Scheme 3.**
Binding Equilibria

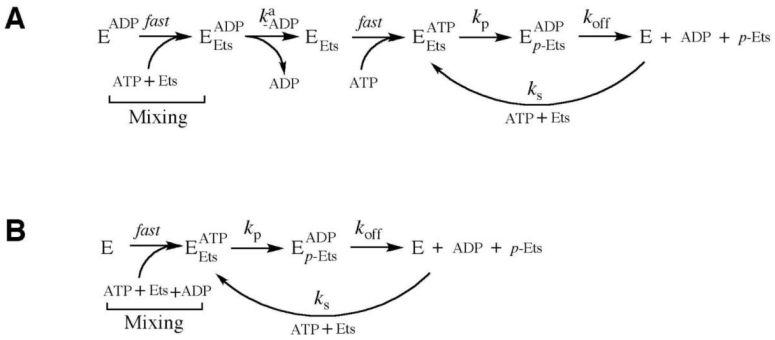


**Scheme 4.**

**A.** ERK2 and ADP are pre-incubated to form the binary complex $E^{ADP}$, before being rapidly mixed with ATP and Ets. **B.** ERK2 is mixed with ATP, ADP, and Ets.

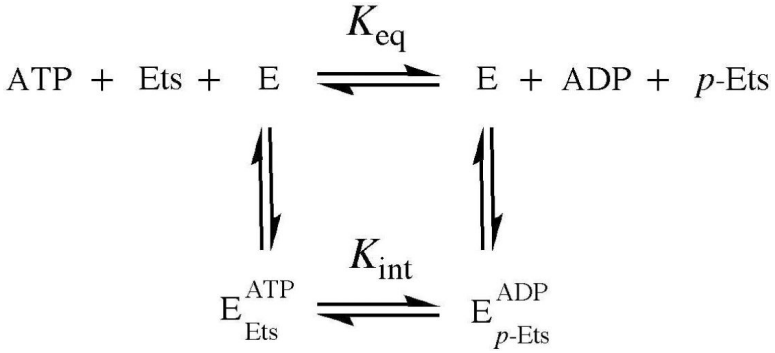


**Scheme 5.**
Reaction Equilibria

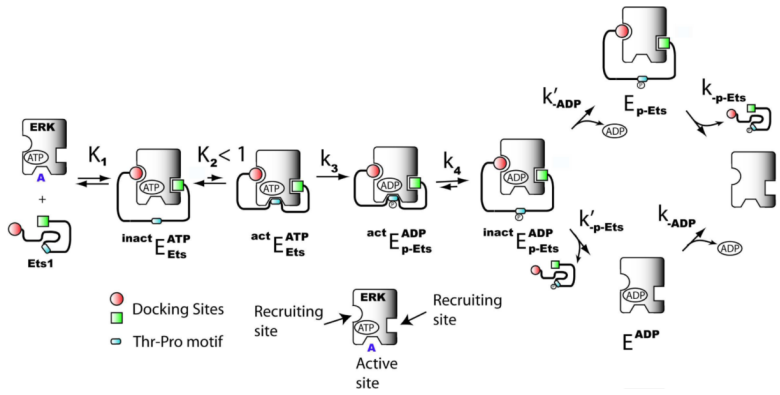


**Scheme 6.**

Kinetic model for the phosphorylation of Ets by ERK2. ERK2 rapidly binds Ets to form an initial complex $^{inact}E^{ATP}_{Ets}$, which is catalytically incompetent, because the Thr-38/Pro-39 motif does not occupy the active site. This complex is mediated by the SAM domain as well as residues in the highly flexible *N*-terminus (21). We propose that $^{inact}E^{ATP}_{Ets}$ is on the reaction pathway for phosphoryl transfer to Thr-38 and that it undergoes an isomerization, to form the activated ternary complex $^{act}E^{ATP}_{Ets}$, which in contrast to $^{inact}E^{ATP}_{Ets}$ is catalytically competent because it is characterized by the binding of the Thr-Pro motif within the active site in such a manner that Thr-38 can hydrogen bond to the catalytic base, Asp-147, priming it for phosphoryl transfer, *k*3 to form $^{act}E^{ADP}_{p-Ets}$, which then undergoes a conformational change, $k_4$, to form $^{inact}E^{ADP}_{p-Ets}$. Product dissociation occurs through a random-order mechanism. *Model terms:* $^{inact}E^{ATP}_{Ets}$, inactive conformation of the ternary complex $E^{ATP}_{Ets}$; $^{act}E^{ATP}_{Ets}$, active conformation of the ternary complex $E^{ATP}_{Ets}$; $^{inact}E^{ATP}_{p-Ets}$ inactive conformation of the ternary complex $E^{ADP}_{p-Ets}$; $^{act}E^{ATP}_{p-Ets}$, active conformation of the ternary complex $E^{ADP}_{p-Ets}$. $K_1$ association constant for the formation of the inactive ternary complex $^{inact}E^{ATP}_{Ets}$; $K_2$ equilibrium constant for the formation of $^{act}E^{ATP}_{Ets}$ from $^{inact}E^{ATP}_{Ets}$; $k_3$ first-order rate constant for the formation of $^{act}E^{ATP}_{p-Ets}$ from $^{act}E^{ATP}_{Ets}$; $k_4$ first-order rate constant for formation of $^{inact}E^{ADP}_{p-Ets}$ from $^{inact}E^{ADP}_{p-Ets}$; $k'_{-ADP}$ first-order rate constant for the dissociation of ADP from $^{inact}E^{ADP}_{p-Ets}$; $k'_{-p\text{-}Ets}$ first-order rate constant for the dissociation of *p*-Ets from $^{inact}E^{ADP}_{p-Ets}$.

## Table 1

Steady-State Kinetic and Thermodynamic Parameters.

| Parameter | Value, Units |
|---|---|
| $k_{cat}^{r}$ | 0.2 ± 0.03 $s^{-1}$[a] |
| $K_{m}^{ADP}$ | 130.0 ± 18 μM[a] |
| $K_{d}^{ADP}$ | 165.0 ± 19 μM[a] |
| $K_{d}^{ADP}$ | 172.0 ± 6 μM[b] |
| $K_{m}^{p-Ets}$ | 13.0 ± 1 μM[a] |
| $K_{d}^{p-Ets}$ | 7.3 ± 0.5 μM[c] |
| $K_{d}^{p-Ets}$ | 16.0 ± 3 μM[a] |
| $k_{cat}^{f}$ | 17.0 ± 3.0 $s^{-1}$[d] |
| $K_{m}^{ATP}$ | 140.0 ± 5.0 μM[d] |
| $K_{i}^{ATP}$ | 65.0 ± 5.0 μM[d] |
| $K_{m}^{Ets}$ | 18.0 ± 2.0 μM[d] |
| $K_{i}^{Ets}$ | 9.0 ± 1.0 μM[d] |

[a] Initial velocities were measured using 50 nM ERK2, 20 mM $MgCl_2$, 2 mM DTT, 0.1–5 mM ADP, and 1.8–90 μM *p*-Ets at pH 7.4, 27 °C, ionic strength 0.15 M (KCl).

[b] Determined by isothermal calorimetry.

[c] Determined by a fluorescence anisotropy competition assay.

[d] Initial velocities were measured using 2 nM ERK2, 20 mM $MgCl_2$, 2 mM DTT, 32–710 μM ATP, and 5.5–100 μM Ets at pH 7.5, 27 °C, ionic strength 0.1 M (KCl).

**Table 2**

Kinetic and Thermodynamic Parameters for the Binding of *p*-Ets-*F*.

| without ADP | | | with ADP | | |
|---|---|---|---|---|---|
| $10^6\, k_{+p\text{-Ets-}F}$ $M^{-1}s^{-1}$ | $k_{-p\text{-Ets-}F}$ $s^{-1}$ | $K_d^{p\text{-Ets-}F}$ μM | $10^6\, k'_{+p\text{-Ets-}F}$ $M^{-1}s^{-1}$ | $k'_{-p\text{-Ets-}F}$ $s^{-1}$ | $K'^{p\text{-Ets-}F}_d$ μM |
| 9.4 ± 0.3[a] | 121 ± 3.8[a] | 12.8 ± 0.6[a, b] | 6.2 ± 0.2[d] | 123 ± 3[d] | 19.8 ± 0.7[d, b] |
| | | 4.8 ± 0.5[c] | 8.2 ± 0.1[e] | 104 ± 2[e] | 12.6 ± 0.6[f, b] |

[a] 20 mM $Mg^{2+}$

[b] calculated from $k_1$ and $k_{-1}$

[c] determined by fluorescence anisotropy

[d] 20 mM $Mg^{2+}$ and 2 mM ADP

[e] 20 mM $Mg^{2+}$ and 4 mM ADP.